RESEARCH ARTICLE | JANUARY 19 2024

Study of material characterization of samarium doped ceria-rice husk ash silica (SDC-RHASiO$_2$) FREE

Zolhafizi Jaidi; Mohd Azham Azmi ✉; Muhammad Akmal Mokhtar; Hamimah Abd Rahman; Shahruddin Mahzan; Azzura Ismail

AIP Conf. Proc. 2925, 020041 (2024)
https://doi.org/10.1063/5.0187751

Study of Material Characterization of Samarium Doped Ceria - Rice Husk Ash Silica (SDC-RHASiO$_2$)

Zolhafizi Jaidi[1,a)], Mohd Azham Azmi[1,b)], Muhammad Akmal Mokhtar[1,c)], Hamimah Abd Rahman[1,d)], Shahruddin Mahzan[1,e)] and Azzura Ismail[1,f)]

[1] *Faculty of Mechanical and Manufacturing Engineering, Universiti Tun Hussein Onn Malaysia, 86400 Parit Raja, Batu Pahat, Johor, Malaysia*

[a)]zolhafizi.jaidi@gmail.com,
[b)] corresponding author: azham@uthm.edu.my
[c)]muhammadakmalmokhtar@gmail.com
[d)]hamimah@uthm.edu.my
[e)]sharudin@uthm.edu.my
[f)]azzura@uthm.edu.my,

Abstract. Additional of metal oxide such as copper oxide, lithium oxide and iron oxide into ceria-based electrolyte had been commercialized to improve the performance of the ceria based material in microstructure modification. In this study, the effect of samarium doped ceria with the addition of rice husk ash silica on its characterization is described. Samarium doped ceria (SDC) with addition of 1.0 wt.% of rice husk ash silica (RHASiO$_2$) was prepared by ball milling method. The SDC-RHASiO$_2$ composite pellets were produced by uniaxial press and were sintered at 700°C. Material characterizations of SDC-RHASiO$_2$ sample were identifying by X-ray diffraction (XRD) for crystalline structures, porosity test and scanning electron microscope (SEM) for surface morphology and microstructures. Based on XRD result obtained, it has been found that the result for SDC-RHASiO$_2$ powder only showed the face-centered cubic lattice structure of ($Sm_{.20}Ce_{.80}O_{1.90}$) without additional impurity phases. SEM micrographs indicated that the porosity percentage decreases when the RHASiO$_2$ was added into SDC. This mixed material is believed could improve the structure as well as the performance of undoped SDC.

INTRODUCTION

The development of intermediate-temperature SOFCs (IT-SOFCs) using novel electrolyte materials is now the main issue facing solid oxide fuel cell (SOFC) technologies in lowering the operating temperature [1, 2]. Gd^{3+} doped CeO_2 (GDC) and Sm^{3+} doped CeO_2 (SDC), among the several forms of ionic oxide conductors, are potential forthcoming alternative electrolytes for these systems because of their high ionic conductivities in a temperature range of 600-800°C [3]–[5]. In comparison to other component materials, the properties of electrolyte powders, such as size, form, crystallinity, compaction, sinterability, etc., should be rigorously regulated [6, 7]. Because of this, it is thought that the creation of ultrafine and homogeneous powders as precursors for the production of dense bulk ceramic electrolytes would significantly affect the densification process, including the sintering temperature and the final electrochemical characteristics [8].

The rice husk, which makes up roughly 23% of the original weight of the rice, is produced as a byproduct of rice beneficiation. For the production of cement, ionic oxide materials, and concrete, this husk can be used as an addition [9]. Thanks to the high silicon concentration, rice husk is now used to manufacture various silicon compounds, including silicon carbide, silicon nitride, and elementary silicon [10]. Due to its high calorific power (about 16720kJ/kg), rice husk is being used more and more as a fuel to generate heat for drying rice. Other than that, previous research had found that small amount of RHA (1wt%-3wt%) can increase the performance of doped ceria [11, 12]. A

Advanced Materials Characterization Techniques 2022
AIP Conf. Proc. 2925, 020041-1–020041-5; https://doi.org/10.1063/5.0187751
Published by AIP Publishing. 978-0-7354-4804-9/$30.00

byproduct of this combustion is rice husk ash (RHA). Rice husk combustion in air always produces silica ash, which can range in colour from grey to black depending on the amount of inorganic contaminants and unburned carbon [9, 10].

Furthermore, despite nanoscale ceria particles appear to have a stronger capacity to sinter than big particles, they also improve the conduction mechanism, limiting the performance of the cell [13]. In order to establish a balance between densification, size, and electrochemical properties, the synthetic approach is crucial for maximising a powder's electrolyte properties. Several procedures can be used to create powders, including hydrothermal treatments, co-precipitation, sol-gel processes, and typical powder mixing and calcination [14, 15].

The approach was chosen because it is a straightforward and inexpensive process, even though the conventional powder mixing and calcination method calls for a number of reaction stages and the addition of dispersants during the compaction of the pellets. Particle size analysis (PSA) and X-ray diffraction (XRD) were used to investigate the micro-sized powders, while scanning electron microscopy (SEM) and energy-dispersive X-ray spectroscopy were used to disclose the sintered bodies (EDX). The purpose of all the experiments was to determine how the addition of rice husk silica affected the SDC.

EXPERIMENTAL PROCEDURES

Sample preparation

Rice husk ash silica ($RHASiO_2$) powder derived from the uncontrolled burning of rice milling at Muar Johor, Malaysia, at a temperature rate of roughly 450ºC with greyish in colour. The powders were ground by ball-milling for 3 hours to obtain the lowest possible particle size (between 0.1µm-0.6µm) before been added into SDC. SDC was obtained commercially (Kceracell, Korea). SDC and $RHASiO_2$ powders were mixed for 2 hours in a low-speed ball-milling method to produce an SDC-$RHASiO_2$ powder comprising 99wt% SDC nanopowders and 1wt% $RHASiO_2$ (lowest composition for $RHASiO_2$ was taken based on previous finding that had been stated in introduction). The SDC-$RHASiO_2$ composite pellets were produced by uniaxial press. Then, the pellets were sintered at 700°C for 60 minutes.

Characterization of samples

The crystalline phases of the samples were characterized by X-ray powder diffractometer, XRD (Shimadzu XRD-6000, D8-Advance, Bruker, German) with Cu Kα radiation (λ=0.15418). The continuous scanning angle, 2θ, set between 20° and 80°, the XRD moves at a speed of 0.02o s^{-1}. Densities of sintered pellets were calculated from the mass and the dimensions of the samples. The cross-sectional morphology of the composite pallets was observed by scanning electron microscope SEM (Hitachi, SU1510, Japan). Energy dispersive X-ray (EDX) was performed to identify the element distribution in the composite.

RESULTS AND DISCUSSION

Phase Analysis

The functional group of alginate and beeswax films were analyzed using FTIR. Figure 2 shows the FTIR spectra for films of 1 wt% and 2 wt% SA. These spectra were used as a reference sample against spectra of alginate and beeswax (1-5 g) films. For films of 1 wt% and 2 wt% SA, broad bands at 3263 cm^{-1} and 3256 cm^{-1} were detected, respectively, contributed by OH stretching band. Small, medium bands were observed at 2936-2937 cm^{-1} in both films, contributed by the presence of -CH stretching vibration band. Stretching bands at 1592 cm^{-1}, 1594 cm^{-1} and 1409 cm^{-1} were due to the existence of carboxylic group as the backbone of SA [10]. The observed band at 1084 cm^{-1} in both films shows the existence of C-C and C-O stretching bands. For films of 1 wt% and 2 wt% SA, the band that recorded the highest intensity was at 1025 cm^{-1} and 1026 cm^{-1}, respectively, which might be due to strong OH binding vibration. Bands observed at 949 cm^{-1}, 811 cm^{-1} and 812 cm^{-1} were contributed by guluronic and mannuronic acids, confirming the existence of G-blocks and M-blocks in SA [10].

X-ray diffraction could be used to determine the phases that are present in commercial powders by analysing their patterns and lattice structures. The X-ray pattern of the composition of SDC and SDC-$RHASiO_2$ pallets can be seen in Figure 1 when the powder is sintered at a temperature of 700°C. During the analysis, there was not a single instance of a secondary phase for $RHASiO_2$ that showed itself on the XRD graph. The analysis for XRD was undergo by using Eva Software to examine the lattice structure, space group and pattern. The lattice structure of ($Sm._{20}Ce._{80}O_{1.90}$) is face-centered cubic with Fm-3m(225) and the peak produce follow the XRD structure for SDC with JCPDS pattern number 01-075-0158. At 700℃, no second phase can be recognized [16]. The $RHASiO_2$ was stay in amorphous state without changing to crystallized during sintering temperature of 700℃. The existence of $RHASiO_2$ had been prove with the result obtain from EDX test.

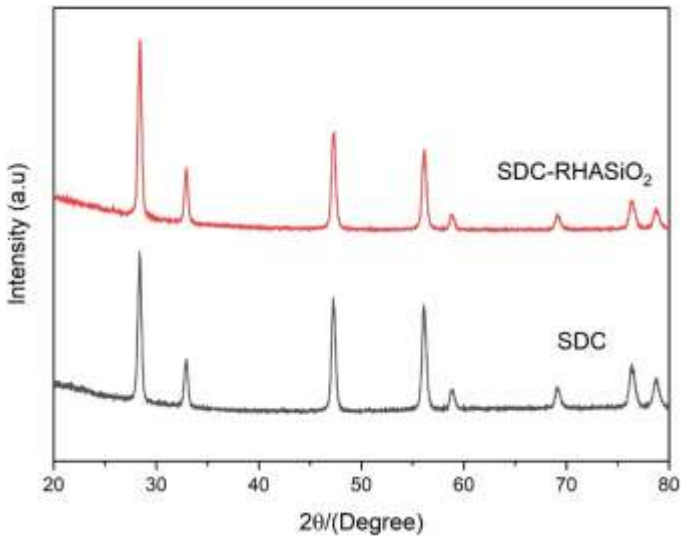

FIGURE 1. XRD patterns of SDC-$RHASiO_2$ composite electrolyte and SDC sintered at 700 ℃

Density and Porosity

The SDC-$RHASiO_2$ pellet was determined by Mettler Toledo Density equipment on findings of porosity and density. The volume of pores that are present in a material is what has been referred to it as porosity, and the density of a material is directly related to the characteristics and performance of powder-compacted elements. The pellet's porosity was measured using the Archimedes principle and distilled water was used as the medium.

TABLE 1. Percentage of porosity and density for all SDC and SDC-$RHASiO_2$

Composition of SDC-$RHASiO_2$ (wt.%)	Sintering Temperature: 700℃	
	Percentage of Porosity (%)	Density, ρ(g/cm^3)
0	41.84	3.9207
1	40.67	3.9847

Table 1 shows the result of the porosity and density examined for the SDC and SDC-$RHASiO_2$ pallets. The pellets are treated to a pressing pressure of three tonnes for three minutes before being sintered at a temperature of 700℃. The result obtained show that SDC pallet has porosity of 41.84% with a density of 3.9207 g/cm^3. On the other hand, the value of porosity for SDC-$RHASiO_2$ was decrease to 40.67%, and density increased to 3.9847 g/cm^3. The porosity

of SDC-RHASiO$_2$ pallet has lower pores composition compared to SDC pallet. This situation proved that the addition of additives strongly promotes the densification of SDC probably due to viscous flow sintering occurs in the Sm-doped ceria system [17].

Morphology Analysis

The cross-sectional morphology of the SDC and SDC-RHASiO$_2$ electrolyte pellet was examined using scanning electron microscopy (SEM). Both pallets were characterized with the magnification of 1000x to observe the porosity structure of cross-sectional morphology pellets. Figure 2 shows the cross-sectional morphology of SDC and SDC-RHASiO$_2$ pellets. The scanning electron microscopy (SEM) reveals a composite microstructure that has a porous surface structure in the areas where it may be identified by darker image. Porosity can be seen more significantly on the images of SEM for SDC compared to SDC-RHASiO$_2$. The result shows that, the porosity percentage decreases when the RHASiO$_2$ was added into SDC. This was verified by the porosity result, which was discussed before.

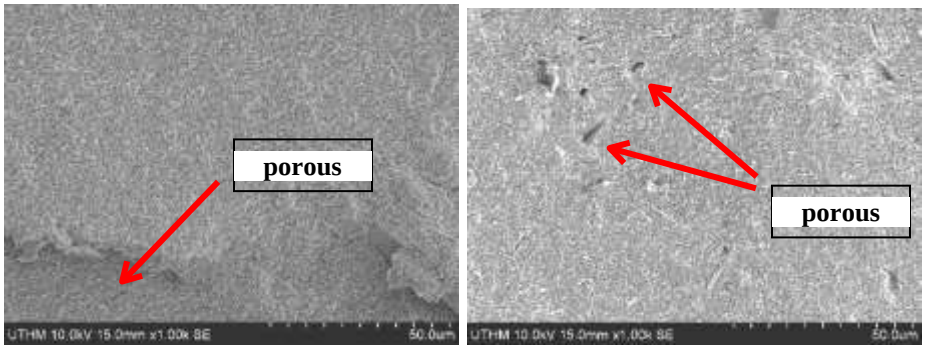

(a) (b)

FIGURE 2. SEM images of (a) SDC and (b) SDC-RHASiO$_2$ pellets with 1000x magnification.

Elemental Analysis

The element distribution of the SDC-RHASiO$_2$ electrolyte of the pellet was shown under the Energy-dispersive X-ray spectroscopy (EDX) machine. Figure 3 shows the distribution element of SDC with the weight of element percentages of oxide, cerium, and samarium with 16.16%, 70.39%, and 13.44% respectively. Figure 4 shows the distribution element of SDC-RHASiO$_2$ 1 wt.% and the composition of elements supposed to exist was on the electrolyte pellets with the weight percentage of element oxide, silica, cerium, and samarium followed by 16.64%, 0.09%, 74.13%, and 9.14% respectively. This result proved that there is SiO$_2$ element detected in the sample which is Si element. The element of SDC-RHASiO$_2$ was stated and the outcome of the experiment conducted meets the desired requirement.

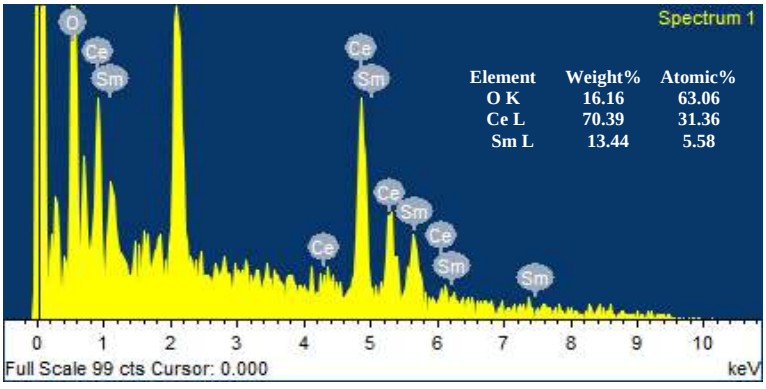

FIGURE 3. EDX distribution for SDC electrolyte pellet

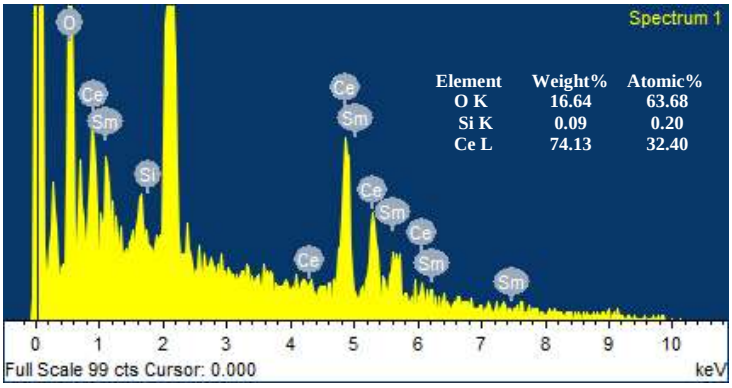

FIGURE 4. EDX distribution element of SDC-RHASiO_2 1% electrolyte pellet

CONCLUSION

This research study is conducted to investigate the characterization of samarium doped ceria with the addition of rice husk ash silica. From these investigations, there is no phase for RHASiO_2. This situation occurs because its stay in amorphous state without changing to crystallized during sintering temperature of 700℃. Other than that, the porosity of SDC-RHASiO_2 pallet has lower pores composition compared to SDC pallet. The porosity also can be seen more significantly on the images of SEM for SDC compared to SDC-RHASiO_2

ACKNOWLEDGEMENT

The authors would like to thank the Ministry of Education Malaysia for supporting this research under Fundamental Research Grant Scheme Vot No. FRGS/1/2020/TK0/UTHM/03/18 and Research Management Centre (RMC), Universiti Tun Hussein Onn Malaysia (UTHM) for managing our research grant.

REFERENCES

1. G. Cai, Y. Gu, L. Ge, Y. Zhang, H. Chen, and L. Guo, Ceram. Int., **43**(12), 8944–8950 (2017).
2. N. Mahato, A. Banerjee, A. Gupta, S. Omar, and K. Balani, Prog. Mater. Sci., **72**, 141–337, (2015).
3 H. C. Lee, J. A. Lee, J. H. Lee, Y. W. Heo, and J. J. Kim, Ceram. Int., **43**(15), 11792–11798 (2017).
4. A. Sawka and A. Kwatera, Ceram. Int., **42**(1), 1446–1452 (2016).
5. W. Wattanathana, C. Veranitisagul, S. Wannapaiboon, W. Klysubun, N. Koonsaeng, and A. Laobuthee, Ceram. Int., **43**(13), 9823–9830 (2017).
6. D. Panthi, N. Hedayat, and Y. Du, ECS Trans., **78**(1), 327–334 (2017).
7. Y. C. Wu, C. H. Chien, and G. Xu, Ceram. Int., **43**, S747–S757 (2017).
8. T. S. Sakthivel, D. L. Reid, U. M. Bhatta B, G. Möbus, D. C. Sayle, and S. Seal, Nanoscale, **7**(12), 5169- 5177 (2015).
9. V. P. Della, I. Kühn, and D. Hotza, Mater. Lett., **57**(4), 818–821 (2002).
10. V. Della, I. Kuhn, D. H.-M. science Forum, and U. 2003, Materials science forum, **416**, 531-536. Transtec Publications; 1999 (2003)
11. Y.M. Su, F.C. Kung, T.L. Su, P.C. Tsai, C.C. Lai and Y.L. Kuo, Journal of the Chinese Institute of Engineers **34(**1), 31-38 (2011).
12. S. Y. Toor and E. Croiset, Ceram. Int., **46**(1), 1148–1157 (2020).
13. L. B. Winck, J. L. de Almeida Ferreira, J. M. G. Martinez, J. A. Araujo, A. C. M. Rodrigues, and C. R. M. da Silva, Ceram. Int., **43**(18), 16408–16415 (2017).
14. G. Dell'Agli, L. Spiridigliozzi, A. Marocco, G. Accardo, D. Frattini, Y. Kwon and S.P. Yoon, Ceram. Int., **43**(15), 12799-12808 (2017).
15. G. Accardo, L. Spiridigliozzi, R. Cioffi, C. Ferone, E. Di Bartolomeo, S.P. Yoon, and G. Dell'Agli, Mater. Chem. Phys., **187,** 149–155 (2017).
16. J. Cheng, C. Tian, and J. Yang, J. Mater. Sci. Mater. Electron., **30**(17), 16613–16620, (2019).
17. Y. Zheng, S. He, L. Ge, M. Zhou, H. Chen, and L. Guo, Int. J. Hydrogen Energy, **36**(8), 5128–5135 (2011).